

Discreteness effects in simulations of hot/warm dark matter

Jie Wang[★] and Simon D. M. White

Max-Planck-Institut für Astrophysik, Karl-Schwarzschild-Str. 1, D-85748 Garching, Germany

Accepted 2007 May 25. Received 2007 May 25; in original form 2007 February 21

ABSTRACT

In hot/warm dark matter (HDM/WDM) universes the density fluctuations at early times contain very little power below a characteristic wavelength related inversely to the particle mass. We study how discreteness noise influences the growth of non-linear structures smaller than this coherence scale in N -body simulations of cosmic structure formation. It has been known for 20 yr that HDM simulations in which the initial uniform particle load is a cubic lattice exhibit artefacts related to this lattice. In particular, the filaments which form in such simulations break up into regularly spaced clumps which reflect the initial grid pattern. We demonstrate that a similar artefact is present even when the initial uniform particle load is not a lattice, but rather a glass with no preferred directions and no long-range coherence. Such regular fragmentation also occurs in simulations of the collapse of idealized, uniform filaments, although not in simulations of the collapse of infinite uniform sheets. In HDM or WDM simulations all self-bound non-linear structures with masses much smaller than the free streaming mass appear to originate through spurious fragmentation of filaments. These artificial fragments form below a characteristic mass which scales as $m_p^{1/3} k_{\text{peak}}^{-2}$, where m_p is the N -body particle mass and k_{peak} is the wavenumber at the maximum of $k^3 P(k)$ [$P(k)$ is the power spectrum]. This has the unfortunate consequence that the effective mass resolution of such simulations improves only as the cube root of the number of particles employed.

Key words: neutrinos – methods: N -body simulations – methods: numerical – dark matter.

1 INTRODUCTION

In the absence of a full analytic understanding of non-linear structure growth, numerical simulations provide a critical link between the weak density fluctuations measured in the cosmic microwave background and the strong inhomogeneities observed on all but the very largest scales in the present Universe. Indeed, numerical simulations played a decisive role in excluding massive neutrinos as a dark matter candidate (White, Frenk & Davis 1983) and in establishing the Λ cold dark matter (Λ CDM) model as the leading and now standard paradigm for the formation of all structure (Davis et al. 1985; White et al. 1987; Cen et al. 1994; Navarro, Frenk & White 1996). With the development of more powerful computer hardware, more accurate numerical algorithms and methods to follow additional physical processes, the importance of simulations as a tool to interpret observations of observed structure continues to increase dramatically. In this paper we are concerned with one aspect of the simplest kind of cosmological structure formation simulation, namely, how discreteness effects can drive the growth of spurious small-scale structure in N -body simulations of evolution from initial conditions containing no such structure.

To create initial conditions for a cosmological simulation, a uniform particle distribution is needed. This can be perturbed by a random realization of the linear fluctuation field associated with the specific structure formation model to be simulated (e.g. Λ CDM). A uniform Poisson distribution of particle positions is not suitable for this purpose, because stochastic ‘root- N ’ fluctuations can exceed the density fluctuations predicted by the desired model over a wide range of scales. To avoid this problem, most early simulations chose a regular cubic lattice as the initial uniform load. Symmetry then assures that there can be no growth of structure in the absence of imposed perturbations (Efstathiou et al. 1985). The preferred directions and the large-scale coherence of the lattice may, however, be a disadvantage, since they can give rise to numerical artefacts. As an alternative, White (1996) suggested using a glass-like initial particle load created by carrying out a cosmological simulation from Poisson initial conditions but with the sign of the peculiar gravitational accelerations reversed, so that each particle is repelled by all the others. When such a system reaches quasi-equilibrium, the total force on each particle vanishes, as for a grid, but there are no preferred directions and no long-range order. The power spectrum on scales much larger than the mean interparticle spacing approaches a power-law $P(k) \sim k^n$ with $n = 4$ (Baugh, Gaztanaga & Efstathiou 1995), where $n = 4$ is the minimal large-scale power expected for a discrete stochastic system (Peebles 1980, section 28).

[★]E-mail: wangjie@mpa-garching.mpg.de

Normally, grid and glass initial loads are considered equivalent. Nevertheless, artefacts due to the initial lattice are obvious in early images of the sheets, filaments and ‘voids’ formed in hot dark matter (HDM) simulations (e.g. Centrella & Melott 1983; Frenk, White & Davis 1984; Efstathiou et al. 1985; Centrella et al. 1988). Baugh et al. (1995) and White (1996) showed that low-density regions appear very different in simulations with a grid initial load than in simulations started from a glass, although Baugh et al. found that this does not show up as a difference in their power spectra. Nevertheless, the regularly spaced clumps seen along filaments in HDM simulations are clearly related to the initial particle grid, and so seem unlikely to reflect a true physical instability. Despite this, Bode, Ostriker & Turok (2001) and Knebe et al. (2003) interpreted analogous structures in their warm dark matter (WDM) simulations (which were set up using a grid initial load) as the result of the physical fragmentation of filaments. The non-linear formation of such small-scale structure could have important consequences in models like HDM or WDM where power on small scales is strongly suppressed in the linear initial conditions. It is thus important to establish which simulated structures are real and which are artefacts, as well as to understand whether the simulations can be improved by, for example, choosing a glass initial load in place of a grid.

Götz & Sommer-Larsen (2002, 2003) carried out WDM simulations using both grid and glass initial loads and reported significant differences. With a grid they found spurious low-mass haloes evenly spaced along filaments, exactly as in earlier HDM experiments. The spacing is simply that of the initial grid, stretched or compressed by the large-scale distortion field. They emphasized, however, that such unphysical haloes were less evident in their simulations starting from a glass. This conclusion disagrees with our own work below, where we find spurious haloes also in simulations from glass initial conditions and with a frequency very similar to that found in the grid case. Curiously, in the glass case also we find the spurious haloes to be regularly spaced along filaments even though the initial condition is *not* regular over the relevant scales.

In this paper, we wish to clarify this issue by isolating the numerical artefact, by exhibiting it in idealized filament formation simulations, by exploring its dependence on the nature of the uniform particle load, and by establishing the dependence of its characteristic scale on the discreteness scale of the simulation and the coherence scale of the WDM/HDM initial conditions. We carry out cosmological simulations of an HDM universe at a wide range of resolutions and with both grid and glass initial loads. In addition, we simulate the collapse of an infinite straight uniform density filament from glass initial conditions, showing that it fragments into regularly spaced clumps. To gain additional insight, we also consider the collapse of a glass to a uniform sheet, and the growth of structure in a uniform, space-filling, but anisotropically compressed glass. Rapid fragmentation on small scales occurs only in the filament case. Our tests also demonstrate that considerable care is needed to produce an initial glass load for which the growth of small-scale structure in filaments is optimally suppressed. We propose a randomization technique which successfully washes out most code-dependent periodic signals in the initial load.

The remainder of our paper is organized as follows. In Section 2 we first discuss the aspects of our simulation code which are relevant to the problem at hand, in particular, how it estimates gravitational accelerations and how it is modified in order to create a uniform glass distribution. We then describe the way in which initial conditions are created for the simulations presented in the rest of the paper. Section 3 presents results from our HDM simulations, showing that all small-scale collapsed structures appear to form initially

as regularly spaced clumps along filaments, and that these are similar for grid and for glass initial loads. Results for our studies of idealized structure formation from anisotropically compressed glasses are presented in Section 4. Rapid fragmentation on small scales occurs only in the filament case. Section 5 examines this filament fragmentation in more detail, showing that its characteristic scale is related to the interparticle separation for a well-constructed glass, but that scales related to the Poisson solver of the glass-construction code can play an important role if their influence is not carefully controlled. Finally, Section 6 summarizes the implications of our results for simulations of structure formation. In particular, we show that for non-linear structures the effective mass resolution of simulations of HDM or WDM universes improves only as the cube root of the number of simulation particles employed. This is much more pessimistic than the direct proportionality to N which might naively have been expected.

2 SIMULATION METHODS AND INITIAL CONDITIONS

All simulations in this paper were performed using the massively parallel N -body code L-GADGET2. This is a lean version of GADGET2 (Springel 2005) with the smoothed particle hydrodynamics part excluded and with the memory requirements minimized. It was originally written in order to carry out the *Millennium Simulation* (Springel et al. 2005).

The computation of gravitational forces is the most critical and time-consuming element of any cosmological N -body code. GADGET2 uses a hybrid tree-PM method where the long-range force is calculated at low resolution using a particle-mesh scheme, and is supplemented by a high-resolution but short-range correction calculated using a tree algorithm. The short-range correction is assembled in real space by collecting contributions from all neighbouring particles. The long-range force is calculated by assigning the particles to a regular cubic mesh, by using Fourier methods to obtain the corresponding potential, and by numerically differencing the result. For a single particle this scheme introduces a maximum force error of 1–2 per cent near the split scale. Choosing a suitable split scale (typically several times the mean interparticle separation) results in force errors for smooth distributions of particles which are almost everywhere far below 1 per cent. GADGET2 uses a space-filling fractal, the Peano–Hilbert curve, to control the domain decomposition associated with parallelization. Because there is a good correspondence between the spatial decomposition obtained from this self-similar curve and the hierarchical tree used to compute forces, it is possible to ensure that the tree decomposition used by the code is independent of the platform, in particular of the number of processors on which it is run. In addition, the ‘round-off’ errors in the forces induced when summing contributions from all processors are explicitly considered. As a result, the forces are independent of the number of processors and the domain cuts that are made. We believe that all code-related numerical effects relating to the calculation of gravitational accelerations are well under control in GADGET2.

Glass construction is embedded in GADGET2 by using some compile options. A preset number of particles is initially distributed at random within the cubic computational volume and the standard scheme is used to obtain the gravitational acceleration on every particle. After reversing the signs of the accelerations, all particles are advanced for a suitably chosen time-step. The velocities are then reset to zero and the whole procedure is repeated. After about a hundred steps the acceleration of each particle approaches zero. Note that this is the acceleration as obtained by the code, including the

effects of force anisotropy, domain decomposition, etc. Because the glass is made in a periodic cube, we can get a large glass file cheaply by tiling a big box with many replications of the original glass. However, the accelerations calculated by the code may no longer vanish exactly for this larger glass because the force anisotropies and inaccuracies now occur on a different scale than when the glass was created.

The FFT calculation and the Barnes–Hut tree used in GADGET2 are both based on static grids. This *spatially fixed* decomposition introduces weak periodic signals in the force calculation, and these are reflected in the particle distribution at the end of the glass-making procedure. We will see below that this can introduce measurable spikes in the 1D power spectrum of the final glass. To reduce such effects we randomly offset the particle distribution in all three coordinates with respect to the computational box before carrying out each force computation during glass making. This suppresses the induced signals quite effectively but does not fully eliminate them. A glass constructed in this fashion is referred to as a ‘good’ glass in the following, while a glass constructed without the random offset technique and showing significant high spikes is referred to as a ‘poor’ glass. In the rest of this paper, we use ‘good’ glasses for our initial conditions except where explicitly noted. These issues are further discussed in Section 5.

Below we consider grid initial loads in addition to glasses in order to compare their performance and to check the results of previous work (Bode et al. 2001; Götz & Sommer-Larsen 2002, 2003). A third quasi-uniform particle distribution, the quaquaversal distribution, has recently been suggested by Hansen et al. (2007) as a non-periodic uniform initial load, a possible alternative to a glass. We have created such a quaquaversal load with 2×8^7 particles using the code provided by Hansen et al. at their web site, and we compare its performance to our grid and glass initial loads in Appendix A. It produces significantly worse discreteness artefacts than either grids or glasses.

Two types of simulation are considered below. The first is a series of cosmological simulations of evolution from HDM initial conditions. Most of these are for a single realization of the HDM density field within a $100 h^{-1}$ Mpc cube, but with different kinds of initial load and with varying mass resolution. One considers a $200 h^{-1}$ Mpc cube in order to better constrain the abundance of large objects. For these simulations, we choose an Einstein–de Sitter universe dominated by a single massive neutrino. We take $H_0 = 76.5 \text{ km s}^{-1} \text{ Mpc}^{-1}$ which implies a neutrino mass of $\sim 55 \text{ eV}$ and a corresponding free-streaming scale $\lambda = 22.2 \text{ Mpc}$ (Bond & Szalay 1983) below which initial fluctuations are exponentially suppressed relative to an assumed $P(k) \propto k$ primordial power spectrum. The power spectrum we actually use to impose fluctuations on our initial loads is based on the theoretical predictions of Bardeen et al. (1986) and agrees with numerical estimates from the Boltzmann solver CMBFAST (Seljak & Zaldarriaga 1996). Since the same realization is used for all our $100 h^{-1}$ Mpc simulations, they should all produce identical structures. We start integrating at redshift $z = 20$ and evolve structure to a formal present-day amplitude of $\sigma_8 = 2$. This corresponds to the collapse of the first non-linear structure in the simulation at $z \sim 6$. As a check of our starting redshift we reran one simulation glass128 starting from $z = 100$. At $z = 15$ the power spectrum of this simulation differed from that of the original run by few per cent or less on all scales.

Our simulations are listed with their parameters in Table 1: pre-IC, L , m_p , ϵ , and n_p denote the initial load, the box size, the particle mass, the softening length and the particle number, respectively.

Table 1. HDM simulations.

Name	Pre-IC	$L(h^{-1} \text{ Mpc})$	$m_p(h^{-1} M_\odot)$	$\epsilon(h^{-1} \text{ Mpc})$	n_p
Glass64	Glass	100	1.06×10^{12}	0.08	64^3
Glass128	Glass	100	1.32×10^{11}	0.04	128^3
Glass256	Glass	100	1.65×10^{10}	0.02	256^3
Glass256-2	Glass	200	1.32×10^{11}	0.04	256^3
Glass512	Glass	100	2.07×10^9	0.01	512^3
Grid128	Grid	100	1.32×10^{11}	0.04	128^3
Qset134	Q-set	100	1.32×10^{11}	0.04	$\sim 134^3$

Our second type of simulation is designed specifically to study the discreteness artefacts which show up in the filamentary structures within our HDM simulations. These simulations follow evolution from a variety of highly idealized initial conditions, all based on uniformly but anisotropically compressed glasses. We consider three different cases.

Anisotropic glass: The glass initial load is compressed by a factor of 2 along one axis, by a factor of 3 along a second axis, and is unaltered along the third axis. Six replications of this configuration are then used to tile the computational cube to produce an initial condition which is uniform and glass-like on large scales but where the forces are no longer balanced on the scale of the interparticle separation.

Sheet: The glass initial load is compressed along one dimension by a factor of 2, so that it fills half of the computational volume. The other half remains empty. This configuration collapses to form an infinite uniform sheet.

Filament: Our glass initial load is compressed by a factor of 2 along two of its periodic directions while the third remains unchanged. The particles then fill a quarter of the computational volume, the rest remaining empty. This configuration collapses to form a uniform straight filament.

All the simulations carried out from these initial conditions assume an Einstein–de Sitter background universe. We define the expansion factor a to be unity at the initial time.

We identify collapsed ‘haloes’ in our HDM simulations using a Friends-of-Friends (FOF) algorithm with linking length 0.2 times the mean interparticle spacing (Davis et al. 1985). In the following we will only consider FOF haloes with 32 or more particles. Subhaloes within these haloes were identified using the SUBFIND algorithm (Springel et al. 2001) with parameters set to retain all overdense self-bound regions with at least 20 particles. Based on these subhalo catalogues we use the techniques of Springel et al. (2005) to construct merging trees which allow us to follow the formation and evolution of all haloes and subhaloes.

3 FILAMENT FRAGMENTATION IN HDM SIMULATIONS

The original motivation for this paper came from an unexpected phenomenon in our HDM simulations. Even when we use a glass initial load, we find that the filaments in these simulations break up into regularly spaced clumps, just as in early simulations based on grid initial loads. We illustrate this in Fig. 1 which shows a slice through simulation glass128. All FOF haloes with $32 \leq N_{\text{FOF}} < 300$ are indicated by red points. It is obvious that many of these low-mass haloes lie in the filaments, and that they are surprisingly regularly spaced along them.

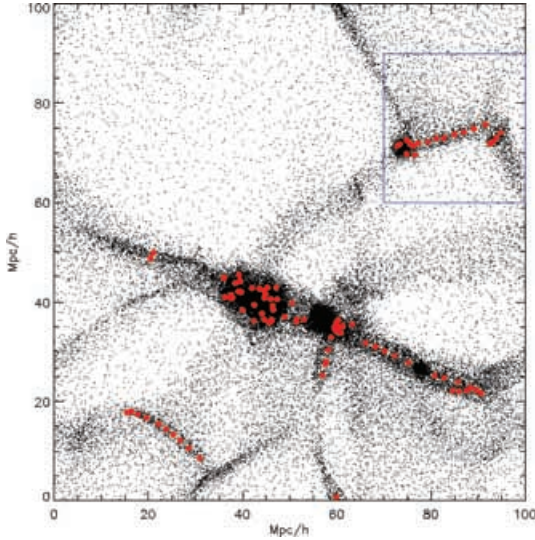


Figure 1. A slice of thickness $10 h^{-1}$ Mpc through the HDM simulation glass128 at $z = 0$. Small black points indicate individual simulation particles, while the larger red points show FOF haloes with $32 \leq N_{\text{FOF}} < 300$.

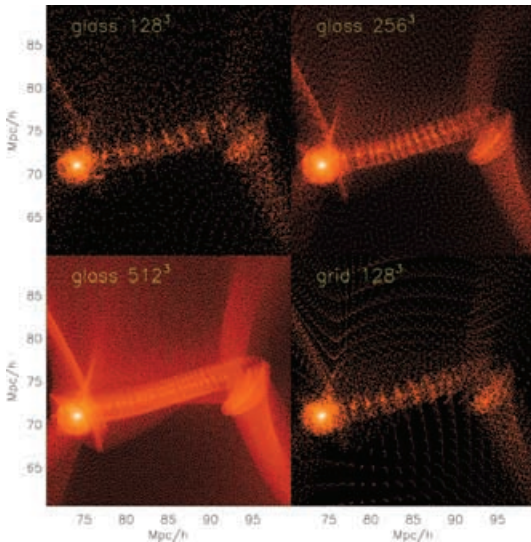


Figure 2. A subregion containing a filament at $z = 0$ in four of our $100 h^{-1}$ Mpc HDM simulations based on differing initial loads and differing mass resolution. The first three panels are taken from glass128, glass256 and glass512, respectively, while the last one (bottom right-hand panel) is taken from grid128. The region shown here corresponds to that surrounded by a blue square in Fig 1.

We find similar behaviour in all our HDM simulations, independent of the initial load and the mass resolution. In Fig. 2 we focus on a small cubic subregion containing a filament. (This region is indicated by a blue square in Fig. 1). In all four simulations, small clumps are visible at regularly spaced positions along the filament. Their spacing is very similar in the two 128^3 simulations, even though one started from a glass and the other from a grid. The spacing is reduced by about a factor of 2 in the 256^3 simulation and by about another factor of 2 in the 512^3 simulation. The clumps are difficult to see in this last case, but this is merely a consequence of the resolution of the image (compare Fig. 3 below). There are strong indications that these clumps are a numerical artefact, not least be-

cause in the grid128 case they line up with the distorted but still recognisable pattern of the initial grid, just as in early HDM simulations (e.g. Centrella & Melott 1983) or in the WDM simulations of Götz & Sommer-Larsen (2003). Götz & Sommer-Larsen (2003) reported that the effect is absent when starting from a glass, although their fig. 1 appears to show it in the filament at the lower right-hand corner of their image. Bode et al. (2001) also noted that many low-mass haloes formed in the filaments of their WDM simulation, but they interpreted this as a result of physical pancake fragmentation. The tight relation between clump scale and mass resolution manifest in Fig. 2 makes it clear, however, that this is actually a reflection of N -body discreteness effects. Its surprising aspect is that the regular clump spacing persists in the glass case where the initial load has no large-scale coherence. We consider this issue further below.

Another consequence of this artefact is illustrated in Fig. 3. It appears that almost all the subhaloes within the massive objects present at $z = 0$ actually originated through spurious filament fragmentation. Fig. 3 focuses on a small subregion of the glass512 simulation which contains the largest FOF halo, an object with several linked density centres at $z = 0$. The lower right-hand panel shows the final mass distribution in this cubic region. All subhaloes with SUBFIND particle count greater than 20 are indicated by blue circles. The other three panels use our merging trees to trace the progenitors of these subhaloes back to earlier times. All of them appear to form initially as evenly spaced ‘beads’ strung along filaments. They later fall into the large halo where they are seen at $z = 0$. The artificial regularity of their formation is illustrated by the two zooms in the upper panels. We conclude that the first generations of haloes in pure HDM or WDM universes should contain no dark matter subhaloes of smaller mass scale.

4 STRUCTURE GROWTH IN IDEALIZED GLASS COLLAPSES

In our HDM simulations there is very little power in the imposed HDM power spectrum below the free-streaming scale. The regular fragmentation of the filaments is clearly related to the mesh for a grid initial load, but the origin of the equally regular fragmentation in the glass case is less obvious. In Fig. 4 we analyse the structure of a ‘good’ 160^3 -particle glass to search for signs of unexpected periodic behaviour. The irregular blue line in this figure is the dimensionless 3D power per unit $\ln k$, $\Delta^2(k) = k^3 P_3(k)$ where $P_3(k)$ is the 3D power spectrum. For comparison, the straight blue line gives the expectation for a Poisson distribution with the same number of particles [$P(k) = 1/N$]. On large scales the power in the glass is far below this white noise level, with $\Delta^2(k) \propto k^7$ rather than $\Delta^2(k) \propto k^3$. For a relatively narrow frequency band near $k = 160$, however, the power is noticeably above the Poisson expectation. This corresponds approximately to the separation of the clumps which form on the filaments so there may be some connection to this artefact in our HDM simulations.

Fig. 4 also shows the power per unit $\ln k$ in 2D and 1D projections of this same glass, $\Delta^2(k) = k^2 P_2(k)$ and $\Delta^2(k) = k P_1(k)$, respectively. Again the measured results are compared to the expectation for a Poisson distribution with the same number of particles. Both cases show features directly analogous to those seen in the 3D power spectrum. On large scales (small k) the power is strongly suppressed relative to the white noise level, with a spectrum which is steeper than white noise by four powers of k . Near $k = 160$ there is a narrow range of wavenumbers where the power rises significantly above the white noise level. Again this feature could be related to the

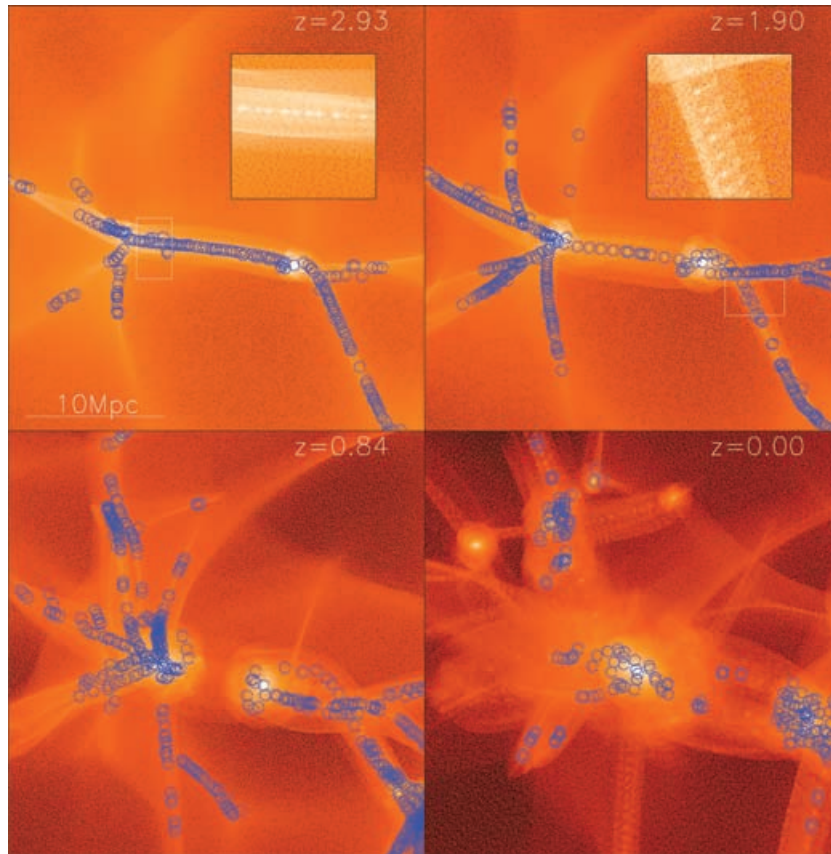


Figure 3. The bottom right-hand panel shows a subregion of glass512 at $z = 0$ containing the largest FOF halo. The blue circles indicate all subhaloes with more than 20 particles within this object. The other three panels show the same subregion at earlier times ($z = 0.84; 1.90; 2.93$) with the blue circles now indicating the progenitors of all the subhaloes identified at $z = 0$. It is striking that almost all these progenitors lie in 1D structures – filaments – at the earlier times. The two smaller plots in the upper panels are stretched and magnified images of the filaments indicated by white rectangles in the main panels.

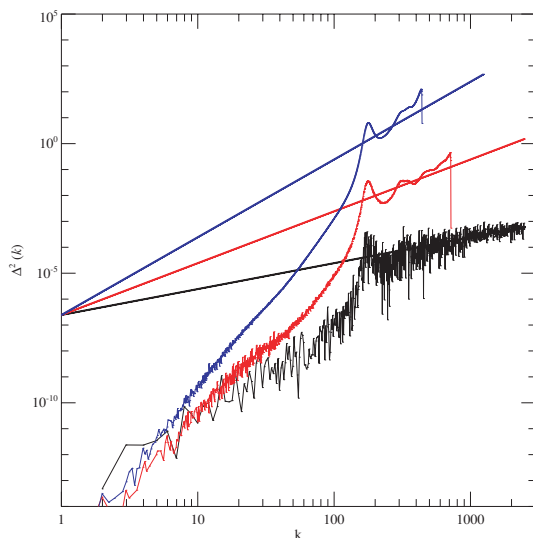


Figure 4. The 1D (black), 2D (red) and 3D (blue) dimensionless power per unit $\ln k$ for a glass with 160^3 particles. The straight lines are the corresponding expectations for a Poisson distribution of 160^3 particles. The wavenumber k is given in natural units so that $k = 1$ corresponds to the fundamental mode of the computational cube. The glass used here is a ‘good’ glass, where random position offsets at each time-step were used to suppress artefacts due to anisotropies in the GADGET2 Poisson solver (see Section 5).

break-up of sheets or filaments into clumps spaced regularly at about the mean interparticle separation.

Whether these features can indeed explain the unexpected fragmentation of filaments in our HDM simulations depends, of course, on how they are amplified as the particle distribution evolves. For the first structures to collapse in an HDM universe, this evolution can be idealized as a succession of three phases (Zel’dovich 1970). During early non-linear growth, the tidal field causes a locally anisotropic flow which first reverses along a single preferred direction while continuing to expand (although at different rates) along the two orthogonal directions. In the second phase, collapse along the preferred axis gives rise to a quasi-2D sheet-like structure, a ‘pancake’. Collapse along one of the other two axes then produces a filament. Finally, material flows along filaments to produce dark matter haloes at their intersections. These features are all clearly visible in Fig. 1, although in practice the different phases overlap and interact significantly. In Fig. 5 we show the results from a set of idealized simulations of anisotropic collapse designed to explore how discreteness noise grows for a glass initial load during these various phases.

To illustrate structure growth in the first of the above phases, the top panel of Fig. 5 shows the evolution of the total 3D power per $\ln k$ for evolution from an anisotropically compressed, but space-filling and otherwise unperturbed glass. (It is easier for us to simulate the isotropic expansion of an anisotropically distorted glass than the anisotropic expansion of an initially isotropic glass.) The 160^3

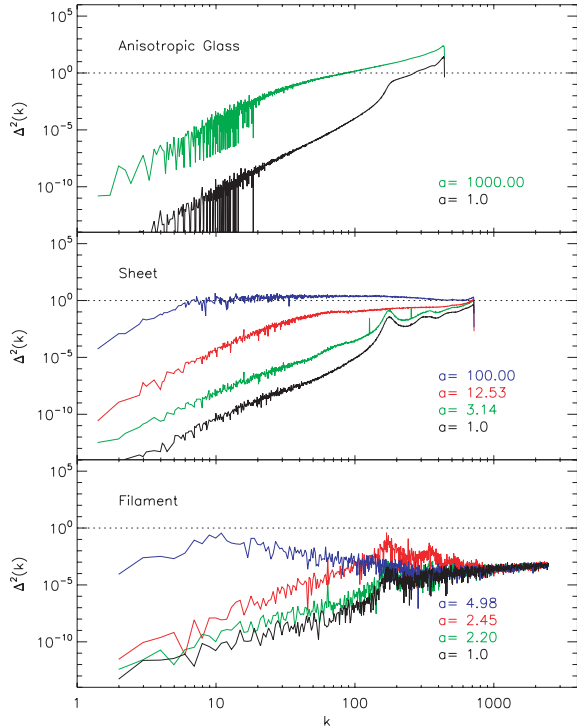


Figure 5. The evolution of the power per unit $\ln k$ in three idealized simulations. Top panel: the 3D power at the initial time and after expansion by a factor of 1000 for an anisotropically compressed but space-filling glass. Middle panel: the 2D power at the initial time and after expansion by factors of 3.1, 12.5 and 100 for the 1D collapse of a compressed glass to a sheet. First collapse occurs at $a = 3.1$. Bottom panel: the 1D power at the initial time and after expansion by a factors of 2.2, 2.4 and 5 for the 2D collapse of a compressed glass to a filament. Here first collapse occurs at $a = 2.2$.

‘good’ glass of Fig. 4 was here compressed by a factor of 2 along the x -axis and a factor of 3 along the y -axis, then replicated six times in order to tile the full simulation cube. The exact periodicities introduced by this procedure are responsible for the regular gaps in power visible at low k in the initial power histogram (the black curve in Fig. 5). It is interesting that the ‘bump’ in power at the discreteness scale is broader than in Fig. 4 and now stretches from near $k = 160$, the interparticle separation of the *original* glass past $k \sim 300$, the interparticle separation of the compressed glass. Clumping during expansion from this initial condition is extremely slow. The green curve shows the power distribution after expansion by a factor of 1000. By this time the matter has aggregated into small dense knots which typically contain 50 particles, but on larger scales the distribution remains almost uniform. At long wavelengths the power has grown by about six orders of magnitude, just as predicted by linear theory. Thus the characteristic mass of the clumps grows as $M_* \propto a^{6/7}$. The amplification of discreteness noise is very weak during the first phase of anisotropic evolution from glass initial conditions.

The second panel of Fig. 5 studies the growth of discrete noise during and after collapse to a sheet. We compress our 160^3 -particle glass by a factor of 2 along one axis, leaving the other half of the simulation cube empty. This initial condition collapses to a thin uniform sheet and thereafter remains thin with the particles oscillating about the symmetry plane. The figure shows the total 2D power per $\ln k$ in the projection of particle distribution on to this plane at four different times: the initial time, the moment when the mass first collapses to a thin configuration ($a = 3.1$), the moment the sheet reaches

minimum thickness for the second time ($a = 12.5$) and a substantially later time ($a = 100$). In this case the power on large scales grows much faster than in the previous case with Δ^2 increasing approximately as a^6 rather than as a^2 . At the time of first collapse, the power in the discreteness peak has grown rather little, even though the power on larger scales has already amplified substantially. By the time of second collapse many non-linear clumps are already evident in the projected mass distribution and the feature at the scale of the initial interparticle separation is no longer visible in the power spectrum. The characteristic non-linear scale is determined by the point where the amplified long-wavelength $\Delta^2 \propto k^6$ tail crosses $\Delta^2 \sim 1$. This scale increases rapidly with time, approximately as $M_* \propto a^3$. Structure in a pancake thus grows by an accelerated version of the standard hierarchical aggregation mechanism illustrated in a more familiar context in the top panel of Fig. 5. Discreteness effects do not appear to play a role other than by setting the initial amplitude of the long-wavelength tail of $\Delta^2(k)$.

The lowest panel of Fig. 5 shows similar data for an idealized simulation of collapse to a filament. We compress our 160^3 -particle glass by a factor of 2 along two orthogonal axes, leaving the remaining three quarters of the simulation cube empty. This bar-like initial condition collapses to a thin, straight filament. The figure shows the 1D power per $\ln k$ for the projection of the particle distribution on to the axis of the filament at four different times: the initial time, the time of first collapse ($a = 2.2$), a time shortly thereafter ($a = 2.4$) and a significantly later time ($a = 5$). The power spectra here are considerably noisier here than in the top two panels because there are far fewer modes per bin in $\ln k$. By first collapse the large-scale power has grown substantially but there is rather little amplification near the discreteness peak at $k \sim 160$. This is similar to the sheet case. Shortly after first collapse, however, the power in the discreteness peak has grown by a large factor, reaching non-linear levels. This shows up as regular clumping along the filament with a periodicity close to $k = 160$. It differs from the behaviour in the sheet case and is apparently analogous to the filament fragmentation we saw in our HDM simulations. We investigate it further in the next section. After the filament collapses the large-scale tail of the power distribution amplifies extremely rapidly, roughly as $\Delta^2 \propto a^{20}$. At the last time plotted this growth is again setting the non-linear scale, as in the upper two panels, and there is no obvious feature near $k = 160$.

In all three of these tests the scale of non-linearity at late times reflects the amplified small- k tail of the initial power spectrum of the glass. This tail grows much more rapidly in a sheet than in a uniform 3D distribution and much more rapidly in a filament than in a sheet. The initial glass, if well made, does exhibit the theoretical minimum power on large scales $P(k) \propto k^4$ (Zel’dovich 1965; Peebles 1980), so that no better suppression of discreteness effects can be hoped for. In the filament case, however, the *first* non-linear structures are clearly different in nature and are related to the interparticle separation scale of the *uncompressed* glass. We now consider this instability more closely.

5 FRAGMENTATION OF FILAMENTS

In Fig. 6 we illustrate the evolution of the collapsing filament discussed in the last section. The first and second columns show projections perpendicular to and along the filament, while the third shows its 1D projected density. Only a tenth of the full length of the filament is plotted in order to make its structure more visible. Shortly after $a = 2$ the filament collapses to minimum thickness and at almost the same time it breaks up into regularly spaced clumps. The clump

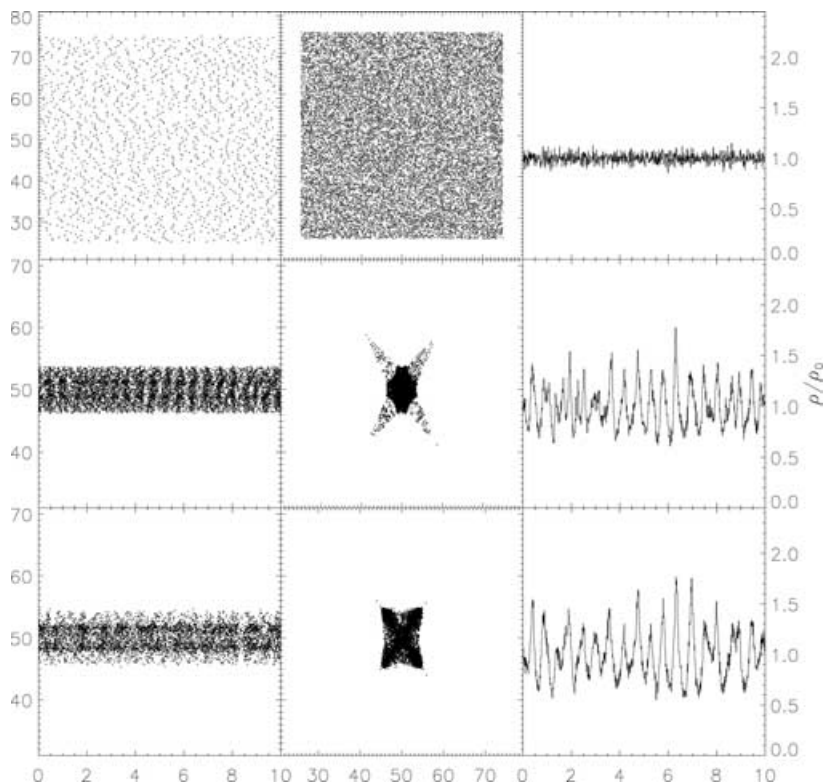


Figure 6. The evolution of an idealized infinite straight filament. The first and second columns are views perpendicular to and along the filament. Comoving coordinates are here normalized so that the side of the computational cube is 100. The third column is the 1D number density profile along the filament. The density is normalized to unity and overdensities should be read off against the scale on the right-hand side of the plot. Results are shown for expansion factors $a = 1, 2.4$ and 2.6 , from the top to bottom panel. For clarity only $1/10$ of the whole filament is shown here. In fact, the total number of clumps lying along the filament is about 160.

spacing is very nearly equal to the mean interparticle separation in the unperturbed glass; we find ~ 160 clumps along the full length of the filament. The number of clumps is independent of the FFT grid used. For 128^3 , 243^3 , 400^3 FFT grids, we find the total number of lumps to be always around ~ 160 . Furthermore, we have repeated this fragmentation experiment with different compression factors in the initial condition. This changes the time of first collapse but it changes neither the fact that the filament breaks up just after first collapse, nor the spacing of the clumps. The same is true even if we adopt different compression factors along the two axes (provided both are well above unity) or if we impose an initial perturbation which is axially symmetric and has no sharp edges. Using an initial glass with a different number of particles produces a change in the interclump separation which scales as the cube root of N . Clearly then, the break-up is associated with a feature of the unperturbed glass.

The regular spacing of these artefacts indicates that modes with $k \sim N^{1/3}$ dominate at least the early non-linear evolution of structure along the filament. This is visible in the left-hand panels of Fig. 7, which repeat the power spectra at the initial time and at $a = 2.4$ (just after collapse) from Fig. 5. At the initial time the power around $k \sim 160$ is more than three orders of magnitude below the threshold for non-linearity, but by $a = 2.4$ it is already approaching unity and is well above the power on all the other scales plotted. This is the reflection in Fourier space of the remarkable regularity seen in Fig. 6. The lower left-hand panel of Fig. 7 plots growth factors for individual modes between the two times. The fastest growing modes have k somewhat smaller than 100, but their growth is insufficient for them to overtake the initial power peak near $k \sim 160$. The power

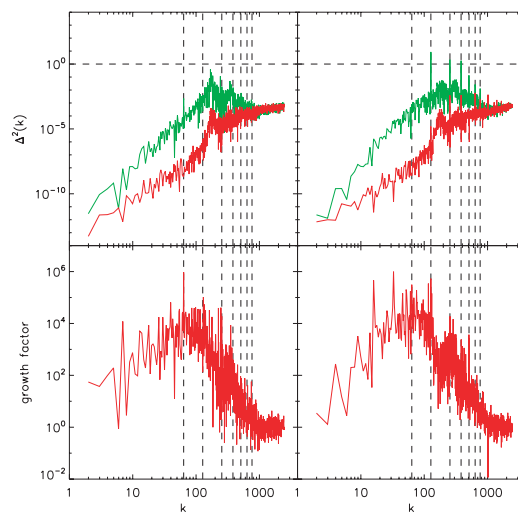


Figure 7. The top panels show the evolution of the 1D power spectra corresponding to the simulations in Fig. 6 (a ‘good’ glass: left-hand side) and Fig. 8 (a ‘poor’ glass: right-hand side) which differ only in the initial glass used. The red curves represent the initial conditions ($a = 1$) while the green curves represent $a = 2.4$. The bottom panels show the growth factors between the two times plotted mode by mode. Note that these reach values in excess of 10^6 . The dashed black vertical lines indicate modes $k = 64, 128, 256, 384, 512, 640, 768$. It can be seen that the growth factors are anomalously high for these modes in both panels, and that in the case of the ‘poor glass’ a number of them are also anomalously high in the initial condition. As a result, at the later time the structure along the filament is dominated in the latter case by the modes with $k = 128, 256$ and 384 .

in all the modes in this peak grows by a similar amount so the peak remains relatively narrow. This causes the regular spacing of clumps along the filament. Tests with a 270^3 -particle glass show identical behaviour but with the peak shifted to $k \sim 270$. We conclude that the regularly spaced clumps which form on the filaments of our HDM simulations are produced by a narrow peak in power near the mean interparticle separation of our initial glass load. This peak is amplified to non-linearity by the remarkably rapid growth of structure which occurs once a filament has collapsed.

Careful examination of Fig. 7 shows that there are particular modes for which the growth appears anomalously strong, notably those with $k = 64, 128, 256, 384, \dots$. This is very likely a consequence of anisotropies in GADGET's Poisson solver which is based on a binary decomposition of the computational volume. For the 'good' glass used here these modes do not grow enough to overtake the power in the peak associated with the interparticle separation, so it is the latter which determines the initial fragmentation scale of the filament. We now show that this is not always the case.

Up to this point all our results have been based on such a 'good' initial glass for which the offset technique discussed in Section 2 was used to minimize features due to anisotropies in the force calculations. Nevertheless, artefacts due to force anisotropies are still visible in some of our plots. For example, spikes can be seen in Fig. 5 at $k = 128$ and 256 in the $a = 3.1$ power spectrum of the sheet (these spikes are solely due to modes with wavevector parallel to the fundamental axes of the computational cube) and at $k = 64$ and 256 in the $a = 2.4$ power spectrum of the filament (see also the left-hand panels of Fig. 7). The growth factors in Fig. 7 show that these 'special' modes grow substantially more rapidly than neighbouring modes. If we do not use random offsets to reduce the impact of algorithmic boundaries in the force calculation, then features of

this kind can be strong enough in the initial glass to significantly affect later evolution. An example is shown in the right-hand panels of Fig. 7 and also in Fig. 8. Here we have carried out exactly the same filament collapse test as before, but using a 'poor' initial glass constructed without using the offset technique. Spikes are now visible at $k = 128, 256$ and 384 in the *initial* 1D power spectrum. These are amplified by the evolution and at $a = 2.4$ the power is dominated by the amplified spike at $k = 128$ rather than by modes in the neighbourhood of the discreteness peak at $k \sim 160$. Spikes at $k = 256$ and 384 are also very strong and several other spikes are clearly visible. As Fig. 8 shows, these spikes cause the filament to break up initially into ~ 128 rather than ~ 160 clumps. Subsequent aggregation into larger objects is similar in the two cases, however, with large-scale effects overwhelming the initial differences.

Eliminating these troublesome power spikes from the initial conditions and from subsequent evolution is not easy. Changing the nominal accuracy of the force calculation affects the amplitude of the spikes but does not remove them. We were surprised to find that similar spikes are present in the initial glass used for the GIF simulations (Kauffmann et al. 1999) even though this was created using a different code based on a P^3M Poisson solver. (For the GIF simulations the artefact was of no consequence, because of the substantial small-scale power imposed in the CDM initial conditions.) The large-scale PM force calculation in both codes imposes a regular 'power of 2' spatial structure, and for GADGET2 this is reinforced by the static Barnes–Hut oct-tree which underlies the calculation of the short-range forces. The unexpected spikes appear to reflect these structural properties of the force construction algorithms. To test this, we projected the initial glass on to periodic directions which are *not* aligned with the axes of the computational box. The corresponding 1D power spectra do not show any sharp spikes.

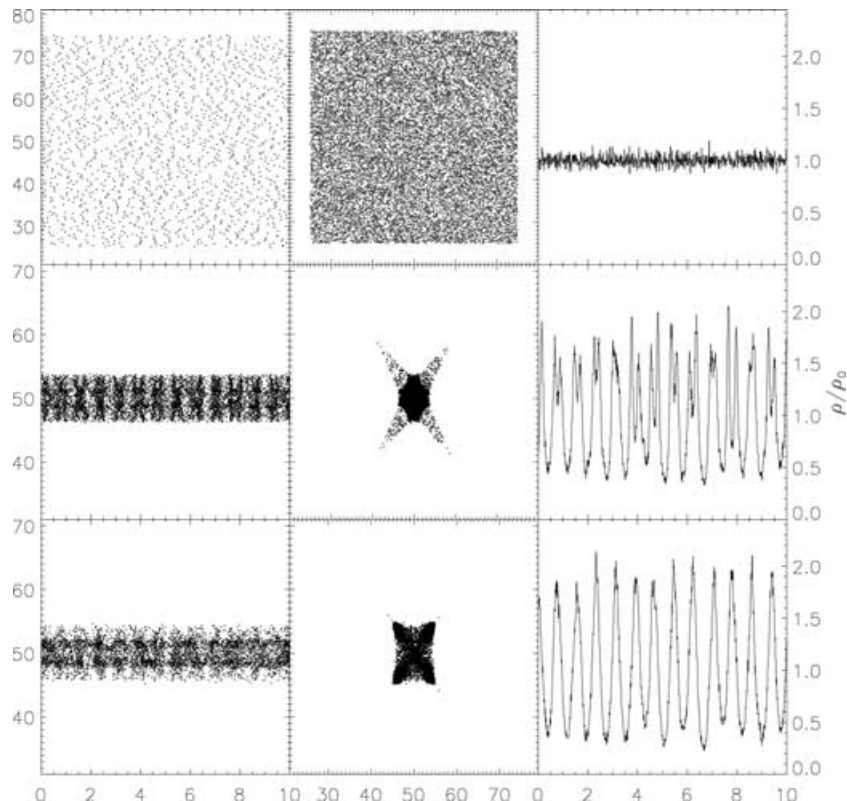


Figure 8. Similar to Fig. 5 but starting from a 'poor' glass where the initial 1D power spectrum shows spikes at $k = 64, 128, 256, \dots$. There are about 128 clumps along the full length of the filament at the last time shown.

The tests in this section demonstrate that even with our random offset procedure, artefacts due to our Poisson solver are not entirely eliminated. On the other hand, these tests are extremely sensitive to such artefacts because of the very high growth rates which occur in the idealized straight filaments we have been studying. While it is clearly important to be aware of the possibility of such numerical effects when simulating WDM or HDM universes, our results here show that for a carefully constructed glass the effects due to the Poisson solver remain subdominant with respect to effects caused by the discreteness of the particle distribution. The latter cannot be eliminated for any choice of initial particle load. They set the fundamental lower limit to the effective resolution of such simulations.

6 DISCUSSION AND CONCLUSIONS

In this paper we have studied how discreteness effects limit the effective mass resolution of N -body simulations of cosmologies like WDM or HDM where structure on small scales is suppressed in the linear initial conditions. Filaments occur in such models as part of the natural development of the cosmic web, but in simulations they fragment into regularly spaced clumps with a separation which reflects the mean interparticle distance in the initial load. These spurious clumps are responsible for all the low-mass substructures we have been able to identify at late times in collapsed haloes. Thus, it appears that in an idealized WDM or HDM universe the first generations of dark haloes are predicted to contain *no* self-bound substructures of significantly smaller scale. Our tests on idealized systems show this fragmentation to occur because 1D projections of a 3D quasi-uniform particle distribution retain substantial power on the scale of the 3D interparticle separation, and this power amplifies very rapidly as the effectively 1D system evolves.

We find (in disagreement with Götz & Sommer-Larsen (2002, 2003)) that spurious fragmentation of filaments occurs in almost identical fashion whether the initial particle load is a glass or a grid. Indeed, as we illustrate in Fig. 9, the effect appears slightly worse for a glass than for a grid. This plot gives mass functions for nine simulations from HDM initial conditions which use different particle numbers and different initial loads. In each case there is a sharp upturn in abundance at small masses which reflects the clumps visible within filaments in Figs 1–3. For initial loads of a given type this upturn shifts to smaller masses by a factor of 2 for each factor of 8 increase in the number of particles. For a given number of particles the upturn clearly occurs at somewhat larger masses in the glass case than in the grid case. Note also that the upturn for the $N = 256^3$ -particle glass simulation in a $200 h^{-1}$ Mpc box agrees very well with that for the $N = 128^3$ -particle glass simulation in a $100 h^{-1}$ Mpc box. This confirms that it is the mean interparticle separation which sets the mass scale, rather than properties of the simulation code or of the particular HDM realization simulated.

If we take the effective lower resolution limit of our HDM simulations to be given by the dashed vertical lines in the lower panel of Fig. 9, we find that it can be expressed as $M_{\text{lim}} = 10.1 \times \bar{\rho} d k_{\text{peak}}^{-2}$, where $\bar{\rho}$ is the mean density of the universe, k_{peak} is the wavenumber at the maximum of $\Delta^2(k)$, the dimensionless power per $\ln k$ in the linear initial conditions, $d = N^{-1/3}L$ is the mean interparticle separation, N is the number of simulation particles and L is the side of the computational box. For our HDM initial conditions $k_{\text{peak}} = 4.23 \times \lambda_{\text{fs}}^{-1} = 0.1 \times (m_\nu/30 \text{ eV}) \text{ Mpc}^{-1}$. The coefficient in our expression for M_{lim} is estimated directly from our HDM results. It may depend significantly on the shape of the primordial power spectrum and so need modification for WDM initial conditions. The scaling $M_{\text{lim}} \propto N^{-1/3}$ should still hold in this case, however. Comparing our formula

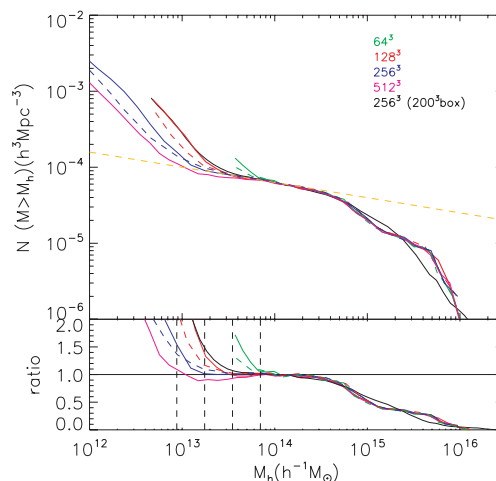


Figure 9. The cumulative halo mass function in eight simulations of an HDM universe. Seven of these start from the same realization of the HDM density fluctuation field within a $100 h^{-1}$ Mpc box, but use different initial particle loads. One follows evolution within a $200 h^{-1}$ Mpc box in order to better constrain the high-mass end of the mass function. Simulations starting from a glass initial load are indicated by solid lines, while those starting from a grid are indicated by dashed lines. The number of particles in each simulation is indicated by labels in the upper panel. The dotted line in this panel is an approximate power-law fit to the low-mass end of the mass function, $N \sim M_h^{-0.2}$, and the lower panel replots the mass functions relative to this power law in order to emphasize the upturn due to discreteness effects. Dashed vertical lines separated by factors of 2 provide a rough indication of the scale where spurious haloes start to dominate in the various cases. The haloes here were identified using an FOF algorithm with $b = 0.2$ (Davis et al. 1985).

without modification to the numerical results of Bode et al. (2001) using $k_{\text{peak}} = 1.0$ and 0.5 Mpc^{-1} , as appropriate for their two WDM models, gives $M_{\text{lim}} = 3 \times 10^{10}$ and $1.2 \times 10^{11} h^{-1} M_\odot$. These values agree well with the upturns in the mass functions which they plot in their fig. 9.

We can also compare with the WDM simulations presented by Knebe et al. (2002, 2003). These authors followed Bode et al. (2001) in arguing that small-mass haloes form along filaments by top-down fragmentation. However, if we compare the mass functions they present for three different simulations in fig. 4 of Knebe et al. (2002) and fig. 3 of Knebe et al. (2003), we find the upturn at low mass for the two simulations with the same numerical resolution but different WDM particle mass to occur at masses which differ by about a factor of 4, while the upturn for the two runs with different numerical resolution but the same WDM particle mass also occur at masses differing by a factor of about 4. This is in roughly agreement with the scaling we predict for M_{lim} and is unexpected for a physical (rather than numerical) feature. We conclude that these results, as well as those of Bode et al. (2001), are consistent with a spurious numerical origin for the low-mass haloes in filaments similar to that we find in our HDM simulations. Furthermore, with our parametrization of the characteristic scale based on the wavenumber at the peak of $\Delta^2(k)$, the dependence of the characteristic mass of the effect on the overall shape of the power spectrum appears to be weak.

This effective resolution limit is unfortunate news for simulations of HDM and WDM universes. In our highest resolution HDM model, for example, the $N = 512^3$ glass simulation of a $100 \text{ Mpc } h^{-1}$ box, the resolution limit is $M_{\text{lim}} = 8.8 \times 10^{12} h^{-1} M_\odot$, which corresponds to a clump of 4300 simulation particles. Thus only haloes

with 5000 particles or more can be considered reliable. This is two or three orders of magnitude below the masses of typical big haloes in the simulation. Contrast this with simulations of CDM universes where the positions, velocities and masses of haloes are reasonably well reproduced even for objects with about 100 simulation particles, giving a logarithmic dynamic range which is about twice as large. Furthermore the effective dynamic range in halo mass increases in proportion to N for CDM simulations, but only in proportion to $N^{1/3}$ in HDM or WDM simulations.

These results are interesting for the question of whether WDM models can reproduce the observed properties of dwarf satellite galaxies in the Milky Way. Available kinematic data for dwarf spheroidals suggest that they are sitting in dark matter haloes with maximum circular velocities of the order of 30 km s^{-1} (e.g. Stoehr et al. 2002; Kazantzidis et al. 2004) corresponding to masses (for an *isolated* object) of about $10^{10} M_{\odot}$. After discounting the spurious low-mass haloes, the mass functions shown in fig. 9 of Bode et al. (2001) demonstrate that haloes of such small mass are not expected for a WDM particle mass of 175 eV and are still strongly suppressed relative to Λ CDM for a mass of 350 eV. We infer that WDM particle masses well in excess of 500 eV will be necessary to produce ‘Milky Way’ haloes with sufficient substructure to host the observed satellites. This is, however, less stringent by a factor of several than constraints based on structure in the Lyman α forest (Viel et al. 2006). It will be interesting to carry out simulations of sufficient resolution to test whether the internal structure of subhaloes in a WDM universe is consistent with that inferred for the haloes of Milky Way dwarfs. The resolution limitations we have explored in this paper imply that, although possible, this will be a major computational challenge.

ACKNOWLEDGMENTS

We thank Volker Springel for help in devising a glass-making scheme which suppresses Poisson-solver-induced power spikes. We thank Adrian Jenkins for the suggestion to consider idealized bar collapses. We thank both of them and also Liang Gao for a number of very useful discussions of the material presented in this paper.

REFERENCES

- Bardeen J. M., Bond J. R., Kaiser N., Szalay A. S., 1986, *ApJ*, 304, 15
 Baugh C. M., Gaztanaga E., Efstathiou G., 1995, *MNRAS*, 274, 1049
 Bode P., Ostriker J. P., Turok N., 2001, *ApJ*, 556, 93
 Bond J. R., Szalay A. S., 1983, *ApJ*, 274, 443
 Cen R., Miralda-Escudé J., Ostriker J. P., Rauch M., 1994, *ApJ*, 437, L9
 Centrella J., Melott A. L., 1983, *Nat*, 305, 196
 Centrella J. M., Gallagher J. S. III, Melott A. L., Bushouse H. A., 1988, *ApJ*, 333, 24
 Davis M., Efstathiou G., Frenk C. S., White S. D. M., 1985, *ApJ*, 292, 371
 Efstathiou G., Davis M., White S. D. M., Frenk C. S., 1985, *ApJS*, 57, 241
 Frenk C. S., White S. D. M., Davis M., 1984, in Setti G., Van Hove L., eds, *Proc. 1st ESO-CERN Symp., Large-Scale Structure of the Universe, Cosmology and Fundamental Physics*. ESO, Garching, p. 257
 Götz M., Sommer-Larsen J., 2002, *Ap&SS*, 281, 415
 Götz M., Sommer-Larsen J., 2003, *Ap&SS*, 284, 341
 Hansen S. H., Agertz O., Joyce M., Stadel J., Moore B., Potter D., 2007, *ApJ*, 656, 631
 Kauffmann G., Colberg J. M., Diaferio A., White S. D. M., 1999, *MNRAS*, 303, 188
 Kazantzidis S., Mayer L., Mastropietro C., Diemand J., Stadel J., Moore B., 2004, *ApJ*, 608, 663
 Knebe A., Devriendt J. E. G., Gibson B. K., Silk J., 2003, *MNRAS*, 345, 1285

- Knebe A., Devriendt J. E. G., Mahmood A., Silk J., 2002, *MNRAS*, 329, 813
 Navarro J. F., Frenk C. S., White S. D. M., 1996, *ApJ*, 462, 563
 Peebles P. J. E., 1980, *The Large-scale Structure of the Universe*. Princeton Univ. Press, Princeton, NJ, p. 435
 Seljak U., Zaldarriaga M., 1996, *ApJ*, 469, 437
 Springel V., 2005, *MNRAS*, 364, 1105
 Springel V., White S. D. M., Tormen G., Kauffmann G., 2001, *MNRAS*, 328, 726
 Springel V. et al., 2005, *Nat*, 435, 629
 Stoehr F., White S. D. M., Tormen G., Springel V., 2002, *MNRAS*, 335, L84
 Viel M., Lesgourgues J., Haehnelt M. G., Matarrese S., Riotto A., 2006, *Phys. Rev. Lett.*, 97, 071301
 White S. D. M., 1996, in Schaeffer R., Silk J., Spiro M., Zinn-Justin J., eds, *Cosmology and Large Scale Structure Formation and Evolution of Galaxies*. Elsevier, Amsterdam, p. 349
 White S. D. M., Frenk C. S., Davis M., 1983, *ApJ*, 274, L1
 White S. D. M., Frenk C. S., Davis M., Efstathiou G., 1987, *ApJ*, 313, 505
 Zel’dovich Ya. B., 1965, *Adv. Astron. Astrophys.*, 3, 241
 Zel’dovich Ya. B., 1970, *A&A*, 5, 84

APPENDIX A: THE QUAQUAVERSAL DISTRIBUTION

Hansen et al. (2007) have suggested using an initial particle load constructed through a simple ‘quaquaversal’ tiling of space (sometimes known as a Q-set). In particular, they suggested using this initial load for WDM simulations. In this appendix, we show what happens if this distribution is used instead of a grid or glass initial load in a number of the tests we have studied in our paper.

A Q-set ‘lives’ in a rectangular box with side ratio $1:1:\sqrt{3}$, and requires a total particle number of the form $N = 2 \times 8^n$ with n an integer. Periodic boundary conditions can be assumed on opposite faces of the box to represent an infinite cosmological distribution. Fig. A1 compares the 3D power spectrum of such a distribution with that of our ‘good’ 160^3 glass. This Q-set has $n = 7$, resulting in a total of $N = 4194\ 304$ particles, and was set up using the codes provided by Hansen et al. (2007). In order to facilitate the comparison we

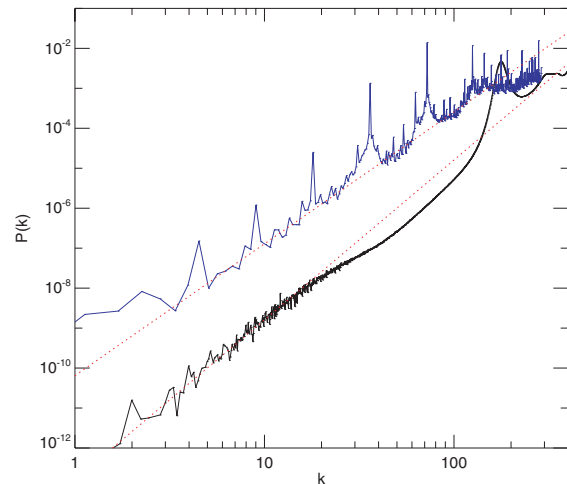


Figure A1. 3D power spectra $P(k)$ for a Q-set (black) and for the ‘good’ $N = 160^3$ -particle glass already used in Fig. 4 (blue). The Q-set has 4194 304 particles in a rectangular box. Its power spectrum is normalized so that its white noise level is at 160^{-3} , just as for the glass. In addition, the units of wavenumber are chosen so that $k = 1$ corresponds to a wavelength 160 times the mean interparticle separation for both distributions. Red dotted lines indicate power laws with slopes 4 and 3.4 which are good fits to the glass and Q-set power spectra, respectively, on large scales.

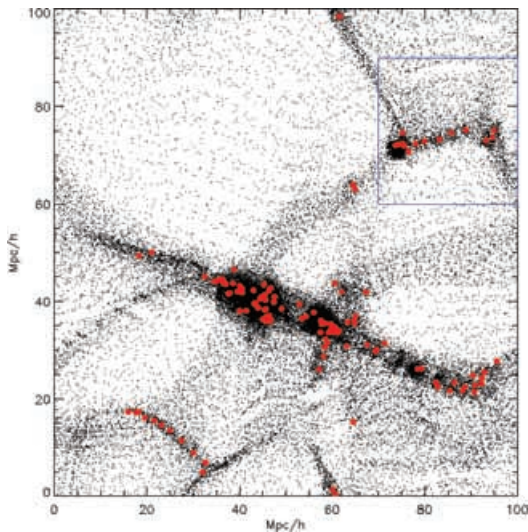


Figure A2. A slice through an HDM simulation directly comparable to Fig. 1, but for a simulation with a Q-set initial load.

shift $P(k)$ for the Q-set so that its white noise level is at 160^{-3} and the mode number $k = 1$ corresponds to a wavelength 160 times the mean interparticle spacing. At all scales significantly larger than the mean interparticle spacing, the power in the Q-set lies well above that in the glass. The mean power declines approximately as $k^{3.4}$ for small k rather than as k^4 , and there is substantial power in a series of additional narrow peaks separated by factors of 2 in k .

We have used this Q-set as the initial particle load for our standard $100 h^{-1}$ Mpc box HDM simulation. Since this simulation is carried out in a cubic region we need to chop off the long end of the Q-set rectangular box leaving a total of $2424\ 140 \sim 134^3$ particles in the simulation. This truncation results in a violation of periodicity in the initial load for one pair of faces of the cubic volume. As a result, spurious small clumps form along this interface during later evolution, but these effects do not propagate into the rest of the simulation. They are not visible in Fig. A2, which is a slice through the simulation to be compared directly with Fig. 1. We exclude a thin slice of the simulation which contains this discontinuity when we calculate the halo mass function at $z = 0$. This is displayed in Fig. A3 and compared to our earlier results.

A comparison of Fig. A2 with Fig. 1 shows that the regularities of the Q-set are much more visually apparent than those of the glass, particularly in low-density regions. The small haloes indicated by red points are again found along filaments and on the outskirts of massive objects. Fig. A3 shows that the Q-set reproduces the halo mass function of our other simulations at high mass, but that the turn-up due to spurious low-mass haloes occurs at significantly higher mass than for glass or grid initial loads. The effective mass resolution of the Q-set simulation is about a factor of 3 worse than in either of the other cases.

We have also carried out our standard idealized filament simulation starting from a compressed Q-set rather than a compressed glass. The particle distribution along a section of the filament is shown just after collapse in Fig. A4 for comparison with the central left-hand panel of Fig. 6. Substantial and regular clumping is seen, although the regularity is considerably more complex (and also stronger) than in the glass case. As in the glass case, the clumps rapidly aggregate into a small number of massive objects during later evolution. The different initial power spectra of the glass and

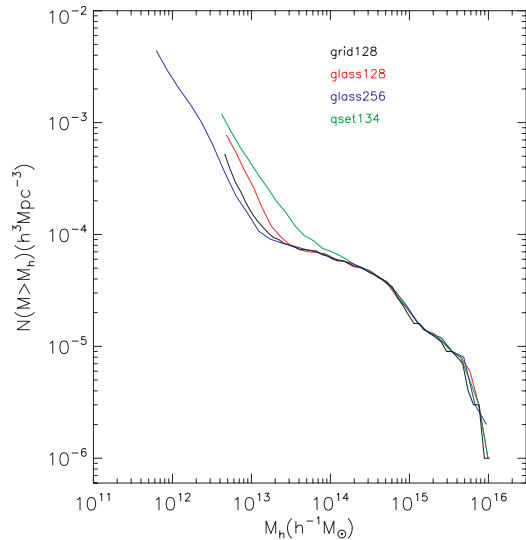


Figure A3. Mass functions for FOF haloes in four HDM simulations started from identical realizations of the HDM fluctuation field but with different initial particle loads. Two start from glass loads with $N = 128^3$ (red) and $N = 256^3$ (blue) and one starts from a grid with $N = 128^3$. All three of these were already shown in Fig. 9. The final simulation starts from a Q-set initial load with $N \simeq 134^3$.

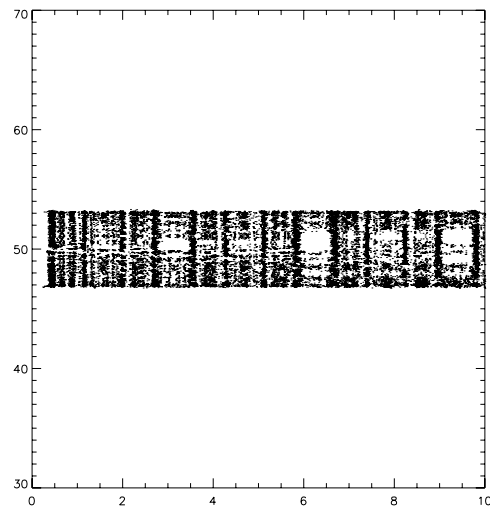


Figure A4. Idealized filament collapse as in Fig. 6 but starting from a compressed Q-set initial condition. The distribution of particles in a section of the filament is shown at $a = 2.2$ and should be compared directly with the middle left-hand panel of Fig. 6.

Q-set cases (Fig. A1), result in different rates of growth of structure along the filament at later times. Structures are always more massive, and are arranged in a more complex pattern along the filament for Q-set than in the glass case.

Our conclusion from these tests is that for given particle number the Q-set performs significantly worse as an initial load than either a grid or a glass. Since the visual regularities it induces are very similar to those seen for a grid and are much stronger than those found with a glass, there does not seem to be any obvious situation where a Q-set would be the preferred choice for an initial quasi-uniform particle load.

This paper has been typeset from a $\text{\TeX}/\text{\LaTeX}$ file prepared by the author.